International Journal of Heat and Mass Transfer 58 (2013) 292–299

Contents lists available at SciVerse ScienceDirect

International Journal of Heat and Mass Transfer

journal homepage: www.elsevier.com/locate/ijhmt

Jet impingement heat transfer on target surfaces with longitudinal and transverse grooves

Yao-Hsien Liu *, Siao-Jhe Song, Yuan-Hsiang Lo

Department of Mechanical Engineering, National Chiao-Tung University, Hsinchu 30010, Taiwan

ARTICLE INFO

Article history:
Received 20 September 2011
Received in revised form 9 November 2012

ABSTRACT

This work reports detailed impingement heat transfer measurements on grooved surfaces using transient liquid crystal method. These grooves are machined on the target surfaces with either parallel or orthogonal to the exit flow direction, and are aligned either with the jet holes (inline pattern) or between the jet holes (staggered pattern). The jet-to-target plate spacing (Z/d) is 3 and the average jet Reynolds numbers are from 2500 to 7700. Results show that heat transfer is enhanced near grooves. However, the grooves underneath the jet holes hinder the impingement flow and the jet impingement heat transfer is reduced. Although local heat transfer shows distinct distributions, there is no significant difference in overall-averaged Nusselt numbers on the grooved surfaces and the highest heat transfer enhancement by grooved surfaces is 15%.

© 2012 Elsevier Ltd. All rights reserved.

1. Introduction

Jet impingement is an effective cooling technique by directing the cooling fluid on the hot target surface. It has been widely applied to the cooling of gas turbine blades, combustion chamber, and electronic components. Jet impingement heat transfer is influenced by many factors such as the jet-to-jet spacing, jet-to-target plate spacing, jet Reynolds number, exit flow directions, and configurations of the roughened surface. In addition, the crossflow development due to spent jet inside impingement chamber shifts the impingement core, and the effectiveness of the impinging jet decreases. Bouchez and Goldstein [1] studied the effect of jet hole diameter on heat transfer due to crossflow effect, and they confirmed that the most effective location was shifted due to crossflow. Moreover, larger jet holes showed higher heat transfer near the inlet of the target surface but gave lower heat transfer near downstream locations due to intensified crossflow. Florschuetz et al. [2] investigated inline and staggered patterns of holes for jet impingement. Results indicated heat transfer is affected by the geometric parameters such as the streamwise/spanwise hole spacing, channel height, and diameter of the jet holes. Extended studies of crossflow have been performed on the heat transfer distribution with and without crossflow by Goldstein and Behbahani [3], and the effect of initial crossflow by Florschuetz et al. [4]. Afterwards, heat transfer and fluid flow characteristics of single and multiple impinging jets were reviewed by Viskanta [5]. Experimental techniques such as the measurement by liquid crystal or infrared camera can provide detailed surface contours and the results help interpret the peak and spatial heat transfer distributions. Huang et al. [6] used transient liquid crystal technique to investigate impingement heat transfer on a target surface with three different exit flow directions. It shows that exit flow direction affects crossflow and alters heat transfer distributions. Ekkad et al. [7] then extended the study to the effect of flow extraction due to film cooling holes on the impinging target surface. A recent survey of the jet impingement cooling for gas turbine blades has been summarized in [8]. Measurement with liquid crystal gives detailed heat transfer distributions and it has been widely applied to related heat transfer research by Stasiek and Kowalewski [9].

Since this paper investigates impingement cooling on the non-smooth surfaces, the following literature survey focuses on the effect of surface roughness. The target surfaces may not be entirely smooth and could also become roughened due to wear, corrosion, or contamination after a period of service. The impingement heat transfer could be enhanced or degraded due to this surface roughness. Gau and Lee [10,11] investigated rib-roughened surfaces under jet impingement. They pointed out that the formation of an air bubble enclosing the cavity due to ribs can prevent the jet from impinging on the wall and reduce the heat transfer. However, some portion of the jet flow in the downstream region, especially when it becomes turbulent, can penetrate the air bubble and impinge, and recirculate inside the cavity, which significantly increases the heat transfer. Taslim et al. [12,13] studied impingement cooling on the gas turbine blade leading edge with ribs and conical bumps. There is a heat transfer enhancement benefit in roughening the surface and conical bumps produce the best heat transfer enhancement. Numerical prediction of multiple jets impinging on the ribbed

* Corresponding author. Address: Department of Mechanical Engineering, National Chiao-Tung University, 1001 Ta-hsueh Road, Hsinchu 30010, Taiwan. Tel.: +886 35712121x55136; fax: +886 35720634.
E-mail address: yhliu@mail.nctu.edu.tw (Y.-H. Liu).

0017-9310/$ - see front matter © 2012 Elsevier Ltd. All rights reserved.
http://dx.doi.org/10.1016/j.ijheatmasstransfer.2012.11.042

Nomenclature

A_j	area of the jet holes (cm^2)
C_d	discharge coefficient of the orifice
d	diameter of the jet hole (cm)
e	depth of the groove (cm)
h	convective heat transfer coefficient ($W\ m^2/k$)
H	distance between the jet hole and target plate (cm)
k	thermal conductivity of acrylic (W m/k)
k_a	thermal conductivity of air (W m/k)
L	thickness of the target plate (cm)
$\dot{m}_j$	jet mass flow rate (kg/s)
Nu	Nusselt number ($=hd/k_a$)
Nu_s	Nusselt number on the smooth surface
p	pitch between the grooves (cm)
ΔP	pressure drop across the orifice plate
Re	average jet Reynolds number ($=\rho V_j d/\mu$)
S	distance between the jet holes (cm)
$T_{w,i}$	initial temperature of the test section (°C or K)
T_w	color change temperature of the liquid crystal (°C or K)
T_m	mainstream temperature (°C or K)
t	transient testing time (s)
V_j	jet velocity (m/s)
X	axial (streamwise) distance of the impingement surface (cm)
Y	spanwise distance of the impingement surface (cm)
Z	distance between the jet hole and target plate (cm)
α	thermal diffusivity of the acrylic test section (m^2/s)
μ	dynamic viscosity of fluid ($N\ S/m^2$)
ρ	density of fluid (kg/m^3)
τ_j	time step (s)

surface was performed by Jia et al. [14]. They found that the ratio between the size of the jets and ribs is the most important since ribs and rib induced recirculation zone prevent the jet flow coming close to the surface. Rhee et al. [15] investigated heat/mass transfer in an impingement/effusion cooling system with ribs. They concluded that using the rib turbulators increases the average heat/mass transfer of 4–11%. Yan et al. [16] and Yan and Mei [17] also measured impingement heat transfer on the target surfaces with ribs. They indicated that the heat transfer may be enhanced or retarded with the presence of the ribs and 45° V-type ribs have the best heat transfer performance. Xing and Weigand [18] studied effect of crossflow schemes on staggered impingement heat transfer with the rib roughened plate. They concluded that the best heat transfer performance is obtained with the minimum crossflow and narrow jet-to-plate spacing no matter on a flat or roughened plate.

Besides ribs, other turbulence promoters with either protrusion or indentation on the surface have also been applied to study impingement heat transfer variations. Azad et al. [19] studied effect of impingement on the surfaces with pin-fins. They found that a pinned surface may produce a higher or lower heat transfer coefficient than a smooth surface, depending on the spent-air crossflow direction. Andrew et al. [20] also investigated impingement heat transfer on the surfaces with rectangular pin-fins. They suggested that the pin-fin array are only worth using with impingement cooling in situations where there is significant cross flow. Hong et al. [21] measured heat/mass transfer in an impingement/effusion system with pin-fins using a naphthalene sublimation method. Results showed the locally low heat transfer regions are reduced and pin fins prevent the wall jet from being swept away, increasing the local heat/mass transfer in the injection region. Azad et al. [22] applied dimples to the target surface and the impingement heat transfer measurement was performed. They concluded that the dimpled surface performed better than the pinned surface at higher Reynolds numbers when the exit flow moves from the nearest exit to the inlet. Ekkad and Kontrovitz [23] also investigated array of jet impingements on the target surface with dimples. They explained that the bursting phenomenon caused by the dimple produces local turbulence, flow separation and reattachment, which breaks up the impingement core and lowers heat transfer level. However, studies of the impingement heat transfer on the grooves surfaces are limited. Sagot et al. [24] measured heat transfer on the grooved circular plates with single impinging jet. Cross-section of the grooves is either square or triangular, and significant heat transfer enhancements up to 81% were obtained as compared with the smooth plate reference case.

In the current study, effects of jet impingement on the surfaces with longitudinal and transverse grooves are studies with the jet Reynolds number of 2500, 5100, and 7700. Literature of heat transfer from arrays of impinging jets on the target surface with grooves is very limited. The detailed heat transfer contours on the target plate are measured by the transient liquid crystal technique, which gives an insight into the impingement heat transfer phenomena. The patterns of the jet arrays and grooves are either inline or staggered, and the heat transfer distribution due to combined effects of impingement flow on the grooves and crossflow can be observed. Comparisons with the literature data are also presented.

2. Experimental setup and procedure

The schematic of liquid crystal thermography setup is shown in Fig. 1. Air is supplied by a roots blower unit. The temperature of the inlet air is heated by a pipe heater and controlled by a temperature control unit. During the heating process, a three-way ball valve is used to divert the air away. The flow is directed into the test section by switching this valve when the preset temperature is reached. The procedure of adjusting the preset temperature is repeated until an acceptable transient testing time is obtained (30–80 s), which gives the initial inlet mainstream temperature of about 55–70 °C for Reynolds numbers of 2500–7700. A CCD camera (Prosilica GigE: GS1380) monitors the color change of the thermochromic liquid crystal coated on the test surface when it

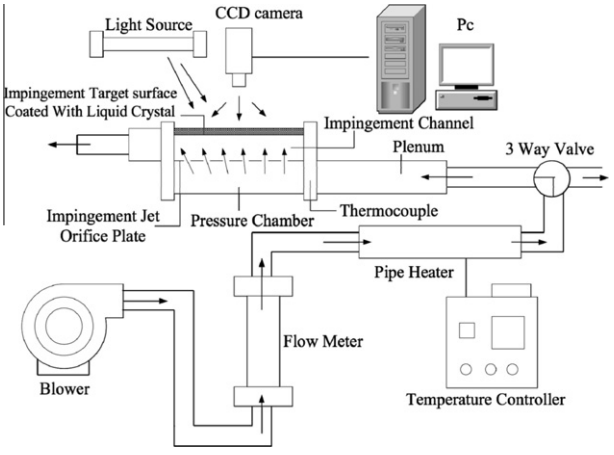

Fig. 1. Schematics of the experimental setup.

reacts to the temperature change. A computer software comes with the CCD camera is used to record the colorful image of the liquid crystal layer and the time during the transient test. The image and the testing time are recorded when the color changes to green (31.2 °C) on the target surface. The measurement region on the target surface contains 1128 × 396 pixels. Airbrush is used to spray the liquid crystal (R30C5W) manufactured by Hallcrest Inc., and the black paint from the same company is also sprayed on the target surface as the background coating. This impingement test section is manufactured from transparent acrylic material as shown in Fig. 2. One orifice plate is sandwiched between the pressure chamber and impingement channel. An array of 4 by 12 rows of circular holes with diameters (d) of 0.5 cm is machined on the jet orifice plate. The thickness of the jet plate is the same as the diameter of the jet hole. The jet-to-jet spacing is 2 cm ($S/d = 4$) and the distance between the jet hole and the target place is 1.5 cm ($H/d = 3$). The cross sectional area of the inlet pressure chamber and the impingement chamber is 2 cm × 8 cm and 1.5 cm × 8 cm, respectively. The plenum, for the flow to develop, has the same cross-section as the pressure chamber and the length is 60 cm. Two thermocouples are instrumented at the inlet of the pressure chamber and the mainstream temperature during the transient test is recorded by Yokogawa Videographic Recorder (MV100). The target plate has the surface area of 24 cm by 8 cm. Therefore, the dimensionless axial distance (X/d) is from 0 to 48 and the dimensionless spanwise distance (Y/d) is from 0 to 16 in the impingement channel. For this setup, the entry flow comes in at $X/d = 0$ of the pressure chamber and it exits at $X/d = 48.0$ of the impingement channel.

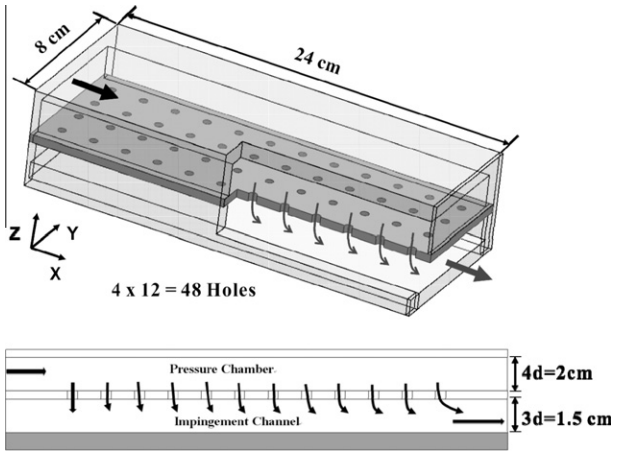

Fig. 2. Drawings of the impingement test section.

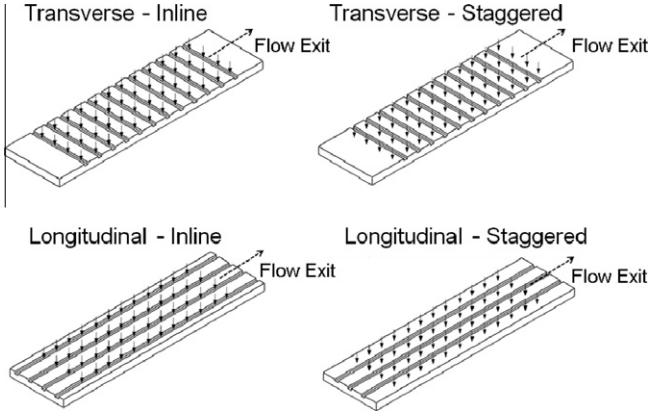

Fig. 3. Groove configurations on the target plate.

Total of four grooved surfaces are fabricated as shown in Fig. 3. The arrows indicate the center locations of the impinging jets when there is no crossflow. The grooves are designed either parallel to the exit flow direction (longitudinal) or orthogonal to the exit flow direction (transverse). The inline pattern demonstrates that the impinging jets are pointing at the grooves, while the staggered pattern demonstrates that the impinging jets are pointing at the locations between the grooves. The grooves have the width of 0.5 cm and the depth (e) of 0.25 cm, and the pitch between the grooves is 2 cm ($p/e = 8$).

3. Heat transfer theory

The one-dimensional semi-infinite transient heat conduction equation based on the convection boundary condition is used to model the heat transfer phenomena occurring on the tested surface:

$$\frac{T_w - T_i}{T_m - T_i} = 1 - \exp\left(\frac{h^2 \alpha t}{k^2}\right) erfc\left(\frac{h}{k}\sqrt{\alpha t}\right) \quad (1)$$

Since the mainstream temperature changes with time, Eq. (1) can be modified using Duhamel's superposition theorem [6] as shown in Eq. (2):

$$T_w - T_i = \sum_{j=1}^{N} \left\{ 1 - \exp\left(\frac{h^2 \alpha (t-\tau_j)}{k^2}\right) erfc\left(\frac{h\sqrt{\alpha (t-\tau_j)}}{k}\right) \right\} [\Delta T_{mj}] \quad (2)$$

where ΔT_{mj} and τ_j are the change of the mainstream temperature and the time-step. The surface temperature is obtained from the liquid crystal layer painted over the target surface. By the measured initial temperature and mainstream temperature, heat transfer coefficient (h) can be calculated. This equation solves every pixels of the captured image and the heat transfer coefficient of each point can be obtained. The non-dimensional Nusselt number is based on the measured convective heat transfer coefficient:

$$Nu = \frac{hd}{k_a} \quad (3)$$

In order to satisfy the semi-infinite solid assumption, the testing time is kept small so that the heat will not penetrate the 1cm-thickness testing plate. The criterion is based on the following equation suggested by Wagner et al. [25]:

$$\frac{\alpha t}{L^2} < \frac{1}{4} \quad (4)$$

A calibration process is performed to obtain the relationship of the color of the liquid crystal with respect to the corresponding temperature. This process begins by spraying the liquid crystal and black paint on a copper plate. Two thermocouples are installed beneath the copper plate and a resistance heater is used for heating. During the heating process, the temperature measured by the thermocouples is recorded and meanwhile the liquid crystal image is taken by the CCD camera. A calibration curve is obtained based on the temperature and the corresponding color of the liquid crystal. This calibration process is carried out under the same conditions as the actual tests. The sources of uncertainties considered in the current study are the mainstream temperature (±0.5 °C), the initial temperature (±0.5 °C), the surface temperature (±0.2 °C), the time during the transient test (±0.2 s), and the material properties. Therefore, the uncertainty of the measured convective heat transfer coefficient (h) is ±10.5% based on Moffat [26].

4. Results and discussion

4.1. Flow rate distribution

Impingement heat transfer on the target plate in this channel is influenced by the flow rate through jet holes. The flow rate through the orifice is calculated based on the following equation:

$$\dot{m}_j = C_D A_j \sqrt{2\rho\Delta P} \tag{5}$$

C_D is the discharge coefficient and A_j is the area of the jet hole. Pressure drop (ΔP) across the orifice plate is measured by the installed pressure taps connected to the micro manometer. By knowing the total flow rate and assuming the density (ρ) and the discharge coefficient are the same for each orifice, the jet flow rate through each jet hole can be determined. The development of the crossflow in the impingement channel is due to spent jet, which is perpendicular to the jet flow direction. The measured jet flow rate and crossflow rate at each location are shown in Fig. 4. It shows that the jet flow rate increases along the axial direction and this trend is consistent with the results based on the same exit flow orientation in the literature. As the jet flow goes into the impingement channel, the crossflow increases along the axial direction and deflects the impinging jets away towards exit flow direction. The ratio of the jet flow rate to the crossflow rate is also presented, which indicates that the effect of jet flow reduces as the crossflow develops downstream.

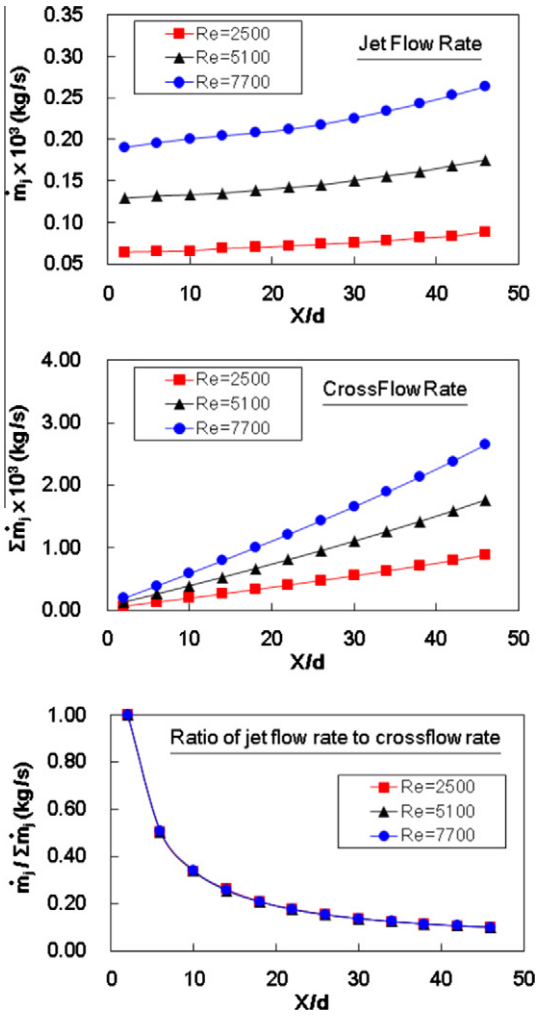

Fig. 4. Jet flow rate and crossflow rate distribution.

4.2. Impingement heat transfer distribution

The focus of this paper is to investigate impingement heat transfer variations due to grooved surfaces. For the detailed heat transfer distribution, axial (or streamwise) locations from X/d = 4.4 to 47.8 are reported at three Reynolds numbers of 2500, 5100, and 7700. This study begins with the measurement of Nusselt number on the non-roughened surface as demonstrated in Fig. 5. Results show that the Nusselt number increases with the jet Reynolds number. As the crossflow rate increases along the axial direction, the effectiveness of the impinging jet reduces and the Nusselt number decreases. Therefore, the highest Nusselt number occurs at small X/d locations and the lowest Nusselt number occurs at large X/d locations. Moreover, the impingement jets tend to be shifted away from the jet hole locations because the crossflow pushes it towards the exit flow direction.

Two categories of grooves are considered in this work: transverse grooves and longitudinal grooves. When the transverse grooves are aligned with the jet holes as shown in Fig. 6, heat transfer inside the groove is reduced. It should be noticed that the data underneath the first hole is not presented, and the crossflow begins to shift the impinging jet away from the grooves. Near the downstream region, the impinging jet is further deflected away due to stronger crossflow effect. The presence of the grooves hinders the jet flow motion. Moreover, transverse grooves induce flow recirculation and it is more difficult for the impingement jet to reach the target surface. Therefore, the Nusselt number outside the groove is higher than the Nusselt number inside the groove for the direct impingement region. When the crossflow rate increases at large X/d, the Nusselt number decreases both inside and outside the grooves. For the staggered arrangement shown in Fig. 7, jet flow is impinging on the surfaces between the grooves. Near the small X/d region, the jet can directly impinge between the grooves due to smaller crossflow effect. It can also be observed that

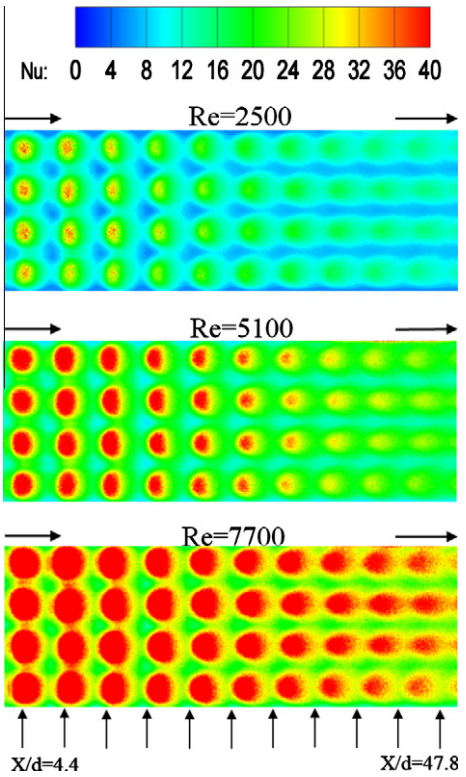

Fig. 5. Detailed Nusselt number distributions on the smooth surface.

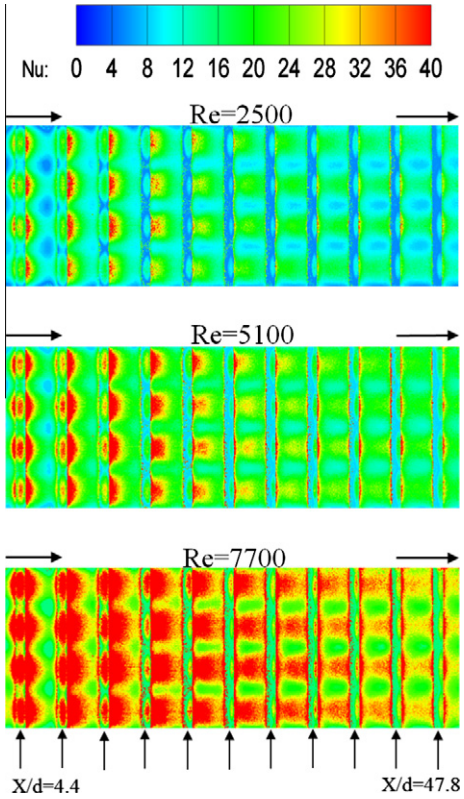

Fig. 6. Detailed Nusselt number distributions for transverse – inline grooves.

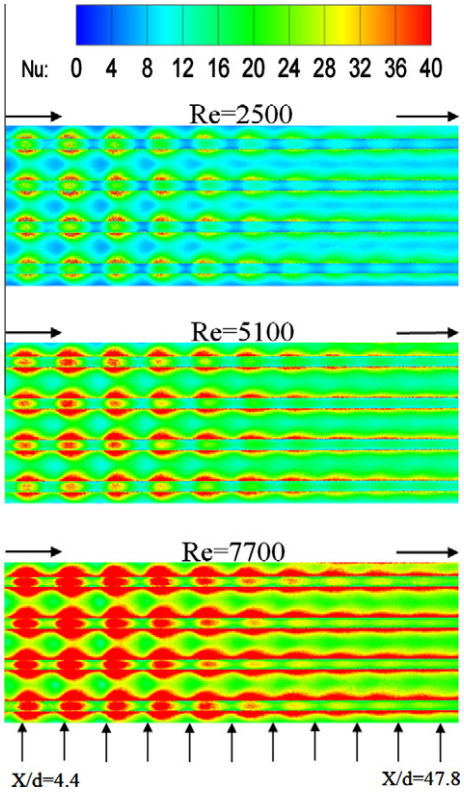

Fig. 8. Detailed Nusselt number distributions for longitudinal – inline grooves.

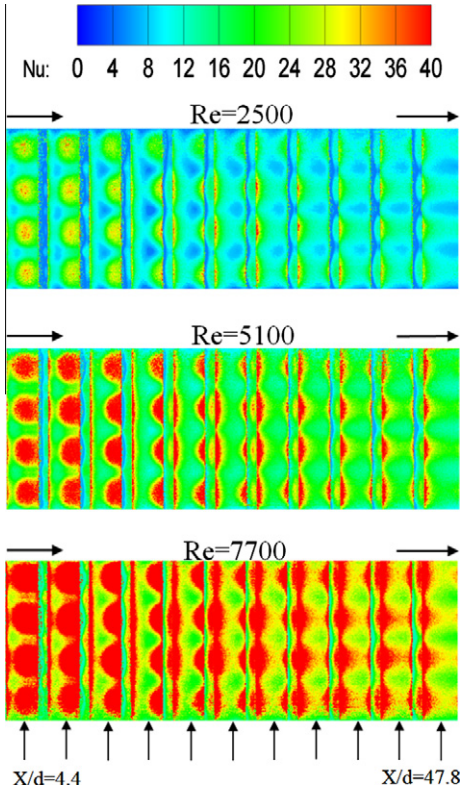

Fig. 7. Detailed Nusselt number distributions for transverse – staggered grooves.

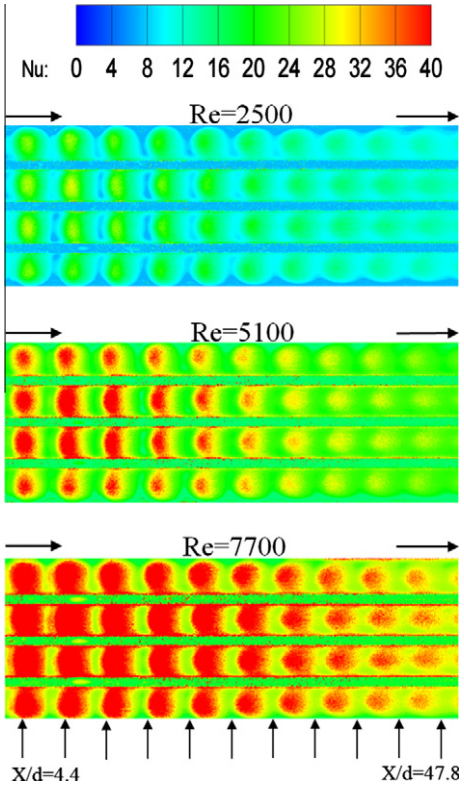

Fig. 9. Detailed Nusselt number distributions for longitudinal – staggered grooves.

impinging jet is pushing away by the crossflow at large X/d locations. For both cases, higher heat transfer is observed on the edge of the grooves due to flow separation and mixing, while heat transfer inside the grooves is relatively smaller. Heat transfer near the downstream region is enhanced due to flow mixing caused by the grooves, and it is higher than the smooth case.

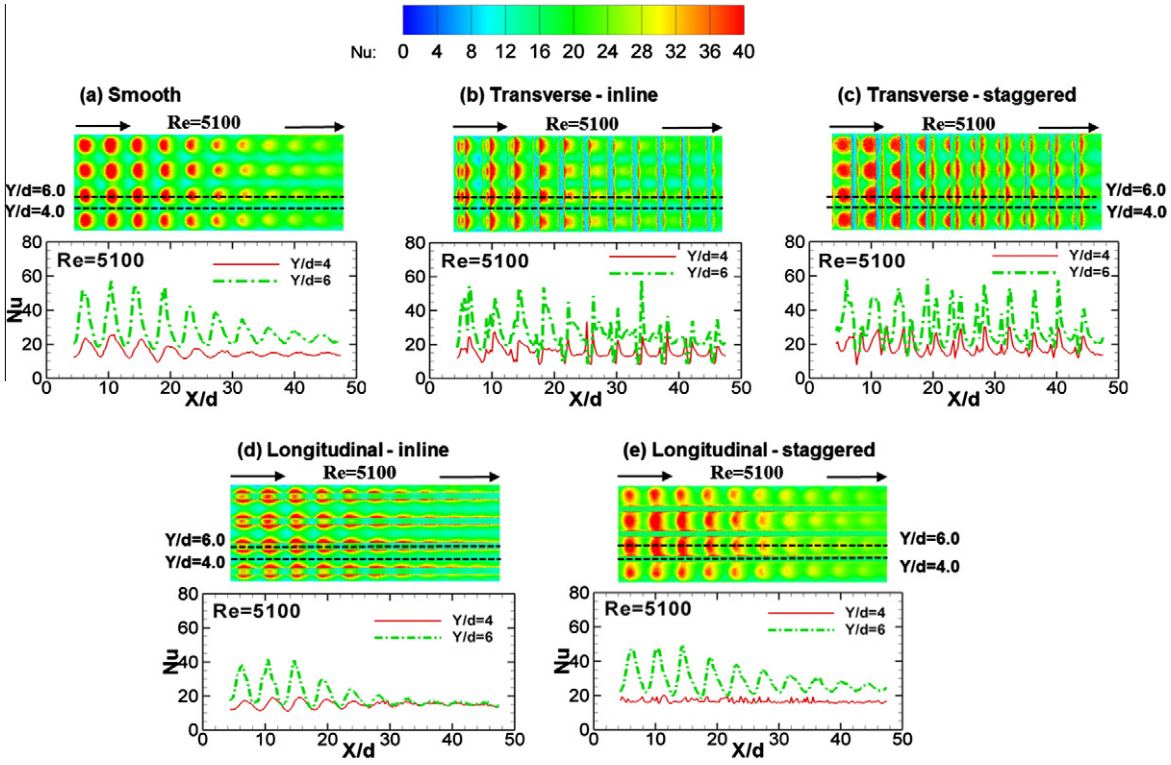

Fig. 10. Nusselt number distributions at $Y/d = 4.0$ and $Y/d = 6.0$.

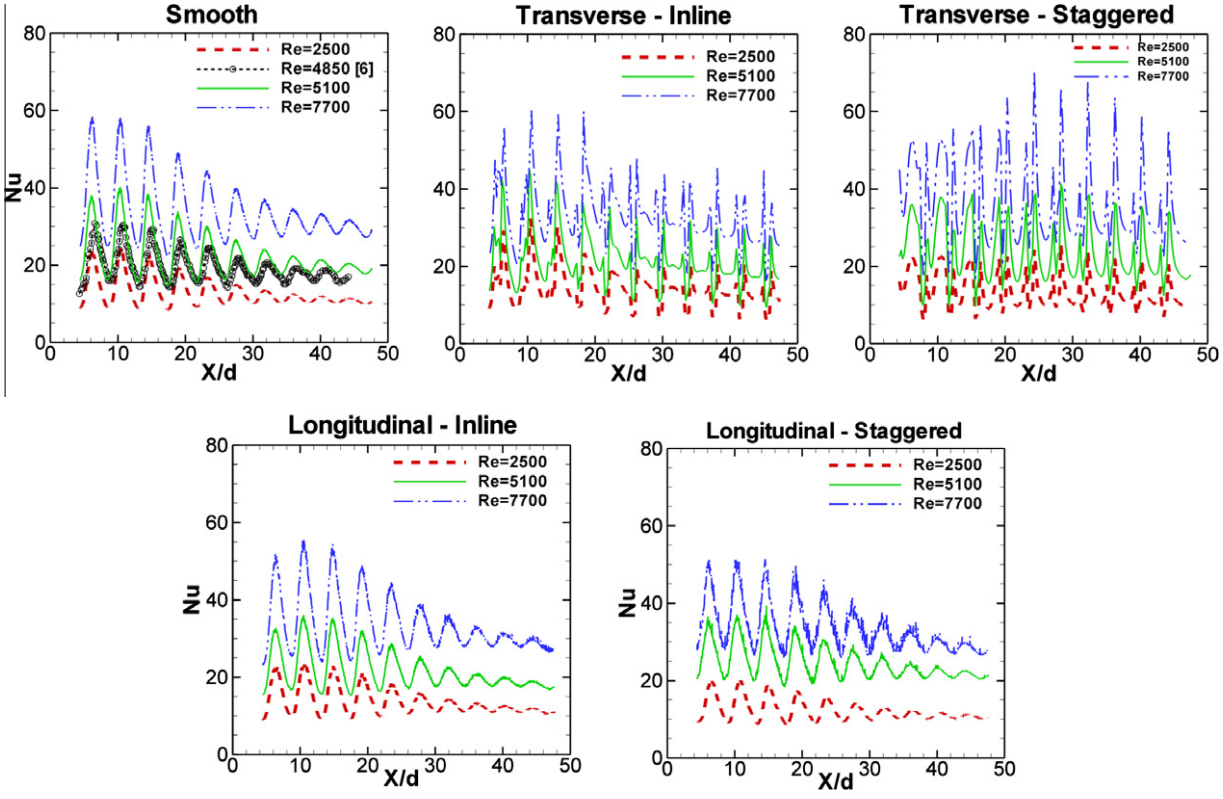

Fig. 11. Spanwise-averaged Nusselt numbers.

When the grooves are designed parallel to the exit flow direction, there is a significant difference in jet flow and crossflow behavior which results in dissimilar Nusselt number distributions. Fig. 8 shows the longitudinal grooves aligned with the jet arrays where the impinging jet directly impinging on the grooves. It clearly shows that the high heat transfer regions underneath jet

holes are affected due to grooves. For the direct jet impingement region, heat transfer inside the grooves is smaller compared to the regions between the grooves. Unlike the transverse grooves, the exit flow now moves both inside and outside the grooves along the axial direction. The crossflow rate inside the grooves increases and the effectiveness of the impinging jets significantly reduces when X/d increases. It is found that Nu value is still higher at the edge of the grooves due to flow mixing caused by the impinging jets and grooves. Fig. 9 shows the longitudinal grooves aligned between the jet holes. Due to the grooves arranged between the impinging jets, partial of the jet fluid moves towards the grooves and the flow reattachment occurs. This phenomena improves the Nusselt number inside the grooves at $X/d = 12.0$. When the flow inside the groove accumulates as the X/d increases, effect of the flow reattachment reduces. The spent jet moves along the axial direction towards the exit and along the spanwise direction towards the grooves. It can be clearly seen that the shape of the impingement region is altered and the Nu value inside grooves is still lower than the impingement region between the grooves. With the grooves arranged between the jets, the impingement heat transfer is altered at larger X/d because partial of the flow moves inside the grooves.

To further interpret the combined effects of jet impingement with grooves, Fig. 10 plots the streamwise distribution of Nusselt number under the jet holes ($Y/d = 6.0$) and between the jet holes ($Y/d = 4.0$) at the jet Reynolds number of 5100. For the transverse grooves shown in Fig. 10(b) and (c), it can be observed that Nusselt number under the jet holes is higher than the Nusselt number between the jet holes. At large X/d locations, Nusselt number is higher than the smooth case due to the enhancement caused by the grooves. For the longitudinal grooves with the inline jet in Fig. 10(d), Nusselt number distribution under the jet holes is relatively higher until $X/d = 30$. Both curves then converge along the axial direction and it demonstrates that the crossflow inside the grooves gets stronger. Therefore, the effectiveness of the impinging jet decreases rapidly along the axial direction. For the longitudinal grooves with the staggered jet arrays in Fig. 10(e), the trend of the Nusselt number distribution for $Y/d = 6.0$ is similar to the smooth case. In this configuration, the Nusselt number under the jet holes ($Y/d = 6.0$) is higher than the Nusselt number between the jet holes ($Y/d = 4.0$).

4.3. Spanwise-averaged and overall-averaged results

Fig. 11 shows the effects of Reynolds number on spanwise-averaged Nusselt number distributions. This average is based on every point along the spanwise direction from $Y/d = 0$ to $Y/d = 16.0$. All cases show that the Nusselt number increases with an increase of the Reynolds number. For this exit flow orientation, the Nusselt number is higher at smaller X/d locations due to smaller crossflow effect. The comparison with the literature data from Huang et al. [6] is plotted for the smooth case and it shows good agreement. For the transverse grooves with the inline jets, it produces similar trends as the smooth case but gives higher Nusselt number at large X/d. For the transverse grooves with staggered jets, the Nusselt number distribution shows similar trend as the inline jets. For the longitudinal grooves, the local peak value of impingement heat transfer is lower than the smooth case at small X/d. The crossflow increases downstream and it is similar to the type of channel flow. Therefore, heat transfer is enhanced due to grooves and it is higher than the smooth surface downstream. Fig. 12(a) presents the overall-averaged Nusselt number for all the cases, based on the data points along the streamwise direction from $X/d = 4.4$–47.8 and the spanwise direction from $Y/d = 0$–16.0. The smooth case is also in good agreement with the literature data from Huang et al. [6]. As the jet Reynolds number increases, the overall-averaged Nusselt number also increases. For both transverse and longitudinal grooves, staggered patterns of the jet holes give slightly higher Nusselt numbers than the inline arrangement at higher Reynolds numbers. As the Reynolds number increases, the difference reduces and all cases have about the same Nu values. The ratio of Nusselt number with grooves to the Nusselt number with smooth surface is also plotted as shown in Fig. 12(b). Heat transfer enhancement and degradation due to addition of grooves is within ±15%. It shows that heat transfer variation due to groove reduces as the Reynolds number increases.

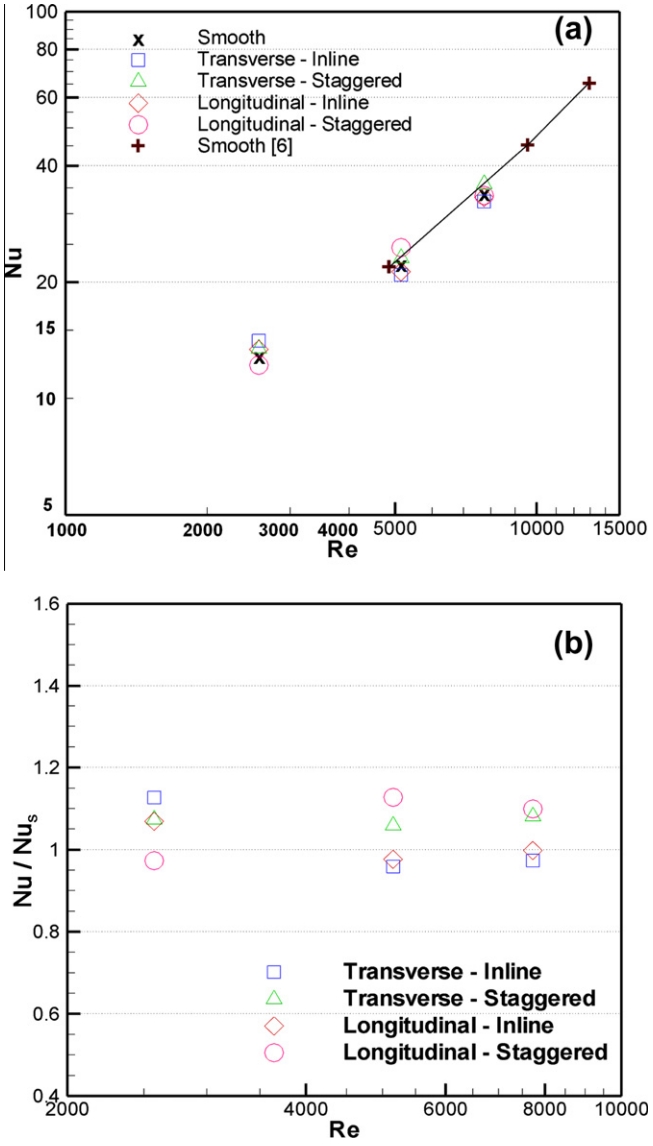

Fig. 12. (a) Overall-averaged Nusselt numbers and (b) ratios of Nu number with groove surface to the Nu number with smooth surface.

5. Conclusion

Experimental studies of impingement heat transfer from jet arrays on grooved surfaces are reported in this paper. Influences of transverse and longitudinal grooves, either inline or staggered to the jet holes, are investigated. Heat transfer measurement by the transient liquid crystal technique shows distinct distributions when compared to smooth surface or other roughened surfaces documented in the literatures. The conclusions can be summarized as follows:

(1) The Nusselt number is higher at small X/d locations near upstream and it decreases along the streamwise directions due to crossflow for both smooth and grooved surfaces.
(2) Impingement heat transfer is reduced when the jets impinging directly on the grooves. When the crossflow dominates downstream, heat transfer is enhanced due to grooves. Higher heat transfer can be observed near the edge of the grooves because of the flow separation and mixing with the jet flow.
(3) For both transverse and longitudinal grooves, the staggered arrangement with respect to the jet arrays show higher Nusselt number than the inline arrangement at higher Reynolds numbers.
(4) The overall-averaged Nusselt numbers on the smooth and grooved surfaces are comparable. It should be noted that this groove configuration may not be the most favorable design and factors such as the exit flow direction or the curvature of the target plate could further contribute to the heat transfer variations.

Acknowledgement

This work has been funded through National Science Council in Taiwan under Contract NSC-98-2218-E-009-016.

References

[1] J.P. Bouchez, R.J. Goldstein, Impingement cooling from a circular jet in a cross flow, Int. J. Heat Mass Transfer 18 (1975) 719–730.
[2] L.W. Florschuetz, C.R. Truman, D.E. Metzger, Streamwise flow and heat transfer distributions for jet array impingement with crossflow, J. Heat Transfer 103 (1981) 337–342.
[3] R.J. Goldstein, A.I. Behbahani, Impingement of a circular jet with and without cross flow, Int. J. Heat Mass Transfer 25 (1982) 1377–1382.
[4] L.W. Florschuetz, D.E. Metzger, C.C. Su, Heat transfer characteristics for jet array impingement with initial crossflow, J. Heat Transfer 106 (1984) 34–41.
[5] R. Viskanta, Heat transfer to impinging isothermal gas and flame jets, Exp. Therm. Fluid Sci. 6 (1993) 111–134.
[6] Y. Huang, S.V. Ekkad, J.C. Han, Detailed heat transfer distributions under an array of orthogonal impinging jets, AIAA J. Thermophys. Heat Transfer 12 (1998) 73–79.
[7] S.V. Ekkad, Y. Huang, J.C. Han, Impingement heat transfer on a target plate with film holes, AIAA J. Thermophys. Heat Transfer 13 (1999) 522–528.
[8] J.C. Han, S. Dutta, S.V. Ekkad, Gas Turbine Heat Transfer and Cooling Technology, first ed., Taylor and Francis, New York, 2000.
[9] J.A. Stasiek, T.A. Kowalewski, The use of thermochromic liquid crystals in heat transfer research, Proc. SPIE – Int. Soc. Opt. Eng. 4759 (2002) 374–383.
[10] C. Gau, C.C. Lee, Impingement cooling flow structure and heat transfer along rib-roughened walls, Int. J. Heat Mass Transfer 35 (1992) 3009–3020.
[11] C. Gau, I.C. Lee, Flow and impingement cooling heat transfer along triangular rib-roughened walls, Int. J. Heat Mass Transfer 43 (2000) 4405–4418.
[12] M.E. Taslim, L. Setayeshgar, S.D. Spring, An experimental evaluation of advanced leading edge impingement cooling concepts, J. Turbomach. 123 (2001) 147–153.
[13] M.E. Taslim, Y. Pan, S.D. Spring, An experimental study of impingement on roughened airfoil leading-edge walls with film holes, J. Turbomach. 123 (2001) 766–773.
[14] R. Jia, M. Rokni, B. Sunden, Impingement cooling in a rib-roughened channel with cross-flow, Int. J. Numer. Methods Heat Fluid Flow 11 (2001) 642–662.
[15] D.H. Rhee, Y.W. Nam, H.H. Cho, Local heat/mass transfer with various rib arrangements in impingement/effusion cooling system with crossflow, J. Turbomach. 126 (2004) 615–626.
[16] W.M. Yan, H.C. Liu, C.Y. Soong, W.J. Yang, Experimental study of impinging heat transfer along rib-roughened walls by using transient liquid crystal technique, Int. J. Heat Mass Transfer 48 (2005) 2420–2428.
[17] W.M. Yan, S.C. Mei, Measurement of detailed heat transfer along rib-roughened surface under arrays of impinging elliptic jets, Int. J. Heat Mass Transfer 49 (2006) 159–170.
[18] Y. Xing, B. Weigand, Experimental investigation on staggered impingement heat transfer on a rib roughened plate with different crossflow schemes, in: Proceedings of ASME Turbo Expo, GT2010-22043, 2010.
[19] G.S. Azad, Y. Huang, J.C. Han, Jet impingement heat transfer on pinned surfaces using a transient liquid crystal technique, Int. J. Rotating Machinery 8 (2002) 161–173.
[20] G.E. Andrew, R.A.A. Abdul Hussain, M.C. Mkpadi, Enhanced impingement heat transfer: the influence of impingement X/D for interrupted rib obstacles (rectangular pin fins), J. Turbomach. 128 (2006) 321–331.
[21] S.K. Hong, D.H. Rhee, H.H. Cho, Heat/mass transfer with circular pin fins in impingement/effusion cooling system with crossflow, AIAA J. Thermophys. Heat Transfer 20 (2006) 728–737.
[22] G.S. Azad, Y. Huang, J.C. Han, Jet impingement heat transfer on dimpled surfaces using a transient liquid crystal technique, AIAA J. Thermophys. Heat Transfer 14 (2000) 186–193.
[23] S.V. Ekkad, D. Kontrovitz, Jet impingement heat transfer on dimpled target surfaces, Int. J. Heat Fluid Flow 23 (2002) 22–28.
[24] B. Sagot, G. Antonini, F. Buron, Enhancement of jet-to-wall heat transfer using axisymmetric grooved impinging plates, Int. J. Therm. Sci. 49 (2010) 1026–1030.
[25] G. Wagner, M. Kotulla, P. Ott, B. Weigand, J. von Wolfersdorf, The transient liquid crystal technique: influence of surface curvature and finite wall thickness, J. Turbomach. 127 (2005) 175–182.
[26] R.J. Moffat, Describing the uncertainties in experimental results, Exp. Therm. Fluid Sci. 1 (1988) 3–17.